Journal of Civil and Environmental Engineering Vol. 56 (2026), No. 2, Special Issues, 63-73

University of Tabriz

Journal of Civil and Environmental Engineering

Floodplain Modeling of the Aji-Chay River within the City Limits of Osku Considering Changes in Bed Geometry, Transversal Structures, and Roughness Coefficient Using the HEC-RAS Model

Yousef Hassanzadeh[a,b,*], Kiyoumars Roushangar[c,d], Mohammad Reza Ahmadzadeh[e], Mehran Hassanzadeh[f,g]

[a] *Professor, Department of Water Engineering, Center of Excellence in Hydroinformatics, Faculty of Civil Engineering, University of Tabriz, Tabriz, Iran*

[b] *Farazab Co. (Consulting Engineers), Research and Writing Capacity Enhancement Affairs, Tabriz, Iran*

[c] *Professor, Department of Water Engineering, Faculty of Civil Engineering, University of Tabriz, Iran*

[d] *Water Science and Hydroinformatics Research Center, Khazar University, Baku, Azerbaijan*

[e] *MSc in Water Resources Engineering and Management, graduated of the Faculty of Civil Engineering, University of Tabriz, Iran*

[f] *Graduated Ph.D. Student, Geotechnical Engineering Department, Faculty of Civil Engineering, University of Tabriz, Iran;*

[g] *Farazab Co. (Consulting Engineers), Dam Department, Tabriz, Iran*

Received: 8 July 2026; **Received in revised form:** 29 October 2026; **Accepted:** 18 November 2026

ABSTRACT:

Flooding, caused by intense rainfall or dam failure, inflicts severe damage on urban, residential, and agricultural areas adjacent to rivers. This study conducts flood hazard mapping for the Aji-Chay River passing through Osku city in East Azerbaijan Province, Iran. A 4.480 km river reach within the city was selected, considering variations in riverbed geometry, transversal structures (bridges), roughness coefficients, and floodplains. Simulations were performed using HEC-RAS 6 with a steady two-dimensional approach. Four bridge spans were analyzed both individually and collectively. The Manning roughness coefficient was determined using the Cowan method, accounting for vegetation cover at selected points. Hydraulic outputs were presented as tables and graphs. Results indicate that the roughness coefficient strongly influences hydraulic parameters, including flow velocity, depth, and flood inundation extent. Using the RAS Mapper environment, the submerged city area relative to total city area was calculated for different return periods. For 100-year, 25-year, and 5-year floods, submersion ratios were 13.21%, 11.66%, and 9.93%, respectively. These values demonstrate that a substantial portion of Osku remains safe from flooding. High-risk zones (inundation depth > 1.5m) cover only about 4% of the city area, primarily along the left bank due to lower elevations. The presence of all four bridges reduces main channel discharge and flood extent compared to a no-bridge scenario. Field evidence and past flood marks validate the model results. The study highlights the need for optimized riverbed management, prevention of buffer zone encroachment, and relocation of critical infrastructure (e.g., fire station) located within the 25-year floodplain.

KEYWORDS:

Floodplain, Transversal structures, Roughness coefficient, Osku city, HEC-RAS

Publisher: Vice Chancellery for Research & Technology, University of Tabriz

https://doi.org/10.22034/CEEJ.2026.73453.2509

Online ISSN: 2717-4077

* Orcid Code Corresponding Author: 0000-0003-4272-4667

E-mail addresses: yhassanzadeh@tabrizu.ac.ir (Yousef Hassanzadeh), kroshangar@yahoo.com (Kiyoumars Roushangar), ahmadzade.reza@gmail.com (Mohammad Reza Ahmadzadeh), mehran.hassanzadeh@gmail.com (Mehran Hassanzadeh).

1. Introduction

Empirical evidence indicates that in various regions of our country, Iran, the majority of destructive flood events in recent years have been caused by cloudbursts, intense rainfall, climate change, and improper human activities. This has resulted in enormous damage to cities, residential areas, and agricultural lands adjacent to flood paths, and has left significant negative impacts on the preservation of the environment and freshwater resources. According to the country's Environmental Protection Organization, of 421 recorded floods between 1951 and 2001, nearly 74% occurred solely between 1981 and 2001. In other words, during the two-decade period from 1981 to 2001, the number of flood occurrences in the country was nearly three times the number of floods occurring between 1951 and 1981, while no significant changes in the country's rainfall patterns have been observed, with only a few exceptional cases. Major causes of flood events include the destruction of forests and rangelands, non-observance of river buffer zones and blockage of river courses, unprofessional construction activities, and severe soil erosion due to prolonged droughts. Therefore, in such areas, estimating, determining, and delineating flood inundation extents in adjacent lands, considering flood discharge with different return periods, is of great importance. This constitutes one of the first steps in determining land use in the region and the type and scale of investment by productive and service sectors in areas adjacent to floodplains. By conducting floodplain mapping of rivers, in addition to estimating potential flood damages for various return periods, it is possible to identify encroachments on the riverbed and floodplain buffer zones and, through implementing necessary measures, prevent further encroachment upon river buffer zones (Hassanzadeh, 2024).

The use of various computer software programs has become essential and common for investigating the effects of river flood events. For this purpose, Kardan et al. (2018); Hassanzadeh et al. (2019), in a study using the CCHE2D software, investigated the hydraulic behavior of the city of Aqqala when exposed to a 100-year return period flood of the Gorgan River. The results indicated that due to the resulting flow pattern and hazard index maps, the complete evacuation of the city is essential. Furthermore, a certain percentage of the city's area is at flood risk, and residents near the watercourse have approximately half an hour to evacuate residential areas from the onset of the flood. Hasanzadeh et al. (2010), in a case study of the Aland River, employed a mathematical method to investigate one-dimensional, non-uniform flow with a mobile bed. The main objective of the research was the numerical modeling of unsteady flow over an erodible bed and the indirect estimation of bed sediment load. In this study, a mathematical model and a modified two-step Van der Veen-Richmeyer method were used. Comparison of model results with experimental data recommended the application of this model for predicting bed profile changes in other rivers, subject to more comprehensive validation in alluvial rivers. Pornaby Darzi et al. (2021), in the Kileh basin of Tonekabon County, determined the flood progression and its height relative to ground elevation for return periods of 2, 5, 25, 50, and 100 years, and produced flood inundation maps. They found that the longer the flood return period, the larger the land area subject to inundation. Eftekhari et al. (2009), in a study aimed at determining flood zones with specified return periods in villages across the entire Gorgan River basin, identified rural areas at flood risk. Using HEC-RAS software, they found that a large number of villages in the region, mostly located in the plain basin with very low slopes, experience flooding and substantial damages due to increased water volume from rainfall or snowmelt. Specifically, 156 villages face high risk, 44 face moderate risk, and 35 face low risk.

The objective of the present study is floodplain mapping of the Aji-Chay River within the city limits of Osku, considering changes in bed geometry, transversal structures, and the roughness coefficient. This research is conducted using the HEC-RAS 6 model and the steady two-dimensional method.

2. Materials and Methods

2.1. Study area

The Aji-Chay River catchment, with an area of approximately 10,500km², is one of the large sub-basins of the Lake Urmia catchment, ranking after the Simineh-Rud and Zarineh-Rud basins in terms of area. Geographically, this basin is situated between longitudes 45°40' and 47°50' E and latitudes 37°40' and 38°28' N in East Azerbaijan Province. The Aji-Chay basin is bounded by the Qarah-Su catchment to the east, the Qezel-Ozan tributaries to the south, the Ahar-Chay catchment to the north, and Lake Urmia to the west, with the general direction of water flow being from east to west. The length of its main river is 265km. The maximum elevation of the Aji-Chay catchment reaches 3,863 meters above sea level on the southern and southwestern slopes of Mount Sabalan (located 25km from Meshginshahr County), while its minimum elevation is 1,270 meters above sea level at the outlet into Lake Urmia. The Aji-Chay River flows through the cities of Sarab, Heris, Bostanabad, Tabriz, Azarshahr, and Osku, respectively. The average annual rainfall in the Aji-

Chay basin over the past ten years is approximately 300mm.

The Aji-Chay River is formed by the confluence of the Biyuk-Chay, Tajyar, Paslar, Razliq, and Vaneq-Chay rivers near the city of Sarab. The study reach is a section of the Aji-Chay branches that flows through the city of Osku, with a length of 4.480 km. Along the studied reach, there are four bridge spans, which have been numbered one through four sequentially from the upstream end of the study reach.

2.2. The HEC-RAS Model

The HEC-2 computer program was designed in 1964 to calculate the characteristics of water flow cross-sections (at the Hydrologic Engineering Center of the US Army Corps of Engineers). The HEC-RAS software is one of the most widely used software programs for modeling river floods and dam breaks, and it enables the evaluation of the effects of influencing factors such as transversal structures intersecting the watercourse. An enhanced version, named the River Analysis System, was later released. This model performs calculations of flow cross-section characteristics for gradually varied flow under both steady and unsteady conditions in rivers and presents the results in graphical and tabular formats. In this research, the HEC-RAS software was used for flood routing, and Arc-GIS software was used for floodplain mapping, delineating flood inundation extents, and identifying high-risk zones. It is worth noting that due to their user-friendliness and widespread applicability, these software programs have been extensively used in river engineering for flood routing on a large scale in numerous projects (Hassanzadeh, 2024).

For the purpose of this study, a steady-state 2D HEC-RAS formulation was employed to simulate the design flood events. This approach was selected to focus on identifying the maximum inundation extent and peak water levels associated with the design return periods (5, 25, and 100 years). Given the relatively slow rising limb of the design hydrographs for the Aji-Chay River, the steady-state approximation provides a conservative and reliable estimation of the peak flood stage. This method allows for a robust assessment of the river's hydraulic capacity and the potential impact of bridge structures on the maximum inundation boundaries in an urban context.

To ensure higher resolution in critical areas, local mesh refinement and breaklines were utilized around bridge piers and abutments to accurately represent the flow contraction. The mesh density was chosen to provide a balance between computational efficiency and the required accuracy for capturing inundation extents in a 4.48km reach.

2.3. Governing equations

The equations employed in the modeling of gradually varied flows include the energy equation and the Saint-Venant equations (continuity and momentum) (Daneshfaraz et al. 2022; Abbaszadeh et al. 2024).

$$y_1 + \frac{V_1^2}{2g} + z_1 = y_2 + \frac{V_2^2}{2g} + z^2 + \sum H_F \quad (1)$$

$$\sum H_F = \sum h_l + \sum h_e \quad (2)$$

where Σhl is the longitudinal energy loss, obtained using the Darcy-Weisbach equation, and Σh_e is the local loss that occurs during flow convergence or divergence, such as when flow passes around bridge piers.

$$h_l = f\frac{l}{d}\cdot\frac{V^2}{2g} \quad (3)$$

$$\frac{\partial Q}{\partial x} + \frac{\partial A}{\partial t} = 0 \quad (4)$$

$$\frac{\partial h}{\partial x} + \frac{V}{g}\frac{\partial V}{\partial x} + \frac{1}{g}\frac{\partial V}{\partial t} = S_0 - S_f \quad (5)$$

In the above relationships, S_0 is the riverbed slope and S_f is the energy grade line slope (Hassanzadeh, 2024).

2.4. Hydrological and morphological data

According to the climatic classification of regions using the Ambrožje method, the city of Osku is located in a cold and dry region. In this study, to delineate the flood inundation extent, digital elevation models (DEMs) with a scale of 1:25000 were obtained from the National Geographical Organization of Iran (Iran National Cartographic Center 2006). The discharge values utilized for the hydraulic modeling specifically 40, 100, and 180 m³/s representing the 5, 25, and 100-year return periods were provided by the East Azerbaijan Regional Water Company. These values are derived from the regional hydrological statistical analysis conducted by the authority, based on long-term historical flow records in the Aji-Chay basin. The selection of these specific return periods (5, 25, and 100 years) was intended to capture a comprehensive range of flood scenarios, from frequent low-magnitude events to extreme, high-impact flood events critical for urban infrastructure and risk assessment.

In terms of morphology, the study reach is considered part of an underdeveloped meandering river, with its meander ratio falling between 1.25 and 2 based on the Cornish classification, which influences the calculation of the Manning roughness coefficient. In this study, the cross-sections of the river under investigation were numbered by the HEC-RAS model starting from the downstream side and were named increasingly according to their distance in meters from the downstream end, as illustrated in Fig. 1.



Fig. 1. Study area

2.5. Determination of the manning roughness coefficient

In this study, according to the morphology of the study reach, the Manning coefficient was initially considered to be 0.05 for the riverbanks and 0.03 for the main channel (Arcement and Schneider 1989). Subsequently, by varying the Manning coefficient values, modeling was performed under steady-state conditions to obtain results in accordance with the items in subsection 2-5-1. Consequently, the results were compared with one another, critical and hazardous conditions were identified, and strategies to prevent or mitigate potential risks were proposed.

Manning's roughness coefficients were determined through a qualitative assessment of the channel morphology and bank vegetation, following standard empirical guidelines for alluvial rivers. This approach ensures that the roughness values are consistent with the observed hydraulic behavior of the Aji-Chay River (United States Geological Survey), as presented in Table 1 (Coon, 1995).

Table 1. Manning roughness coefficients for the riverbed and banks

River section	Coefficient type						
	n_b	n_1	n_2	n_3	n_4	m	n
River channel	0.30	0.016	0.012	0.012	0.01	1.15	0.092
left and right banks of the river	0.05	0.020	0	0.025	0.007	1.15	0.1173
the channel at the 5 downstream reaches	0.03	0.016	0.012	0.013	0.013	1.15	0.0966

To account for the spatial heterogeneity of the river reach, different Manning's roughness coefficients were assigned to the main channel and the banks. The main channel was assigned a lower roughness coefficient to represent the relatively smooth bed material, while higher values were applied to the banks to account for the increased hydraulic resistance caused by [e.g., riparian vegetation and irregular land surfaces]. This approach, based on Cowan's classification, ensures that the model captures the physical reality of the flow resistance in a multi-land-use environment. Furthermore, the sensitivity of the inundation extent and water surface elevation to these roughness assignments was considered to ensure the reliability of the predicted flood patterns.

The Cowan equation is as follows:

$$n = (n_b + n_1 + n_2 + n_3 + n_4)m \quad (6)$$

In this equation, n_b is the base Manning coefficient based on the grain size distribution of the channel bed material, which ranges approximately between 2 and 64mm. n_1 represents the degree of surface irregularity of the watercourse or floodplain, n_2 accounts for cross-section shape variations, n_3 corresponds to obstructions in the watercourse or floodplain, n_4 reflects the vegetation cover of the watercourse or floodplain, and mm is the correction factor for the meandering pattern of the river channel. According to the recommendation of the United States Geological Survey, mm is taken as unity when water flow enters the floodplain (USBR 1988). However, in accordance with Table 5-7 of Publication No. 688 (Planning and Budget Organization 2022) of the Planning and Budget Organization of Iran, and considering the meandering ratio obtained for the study reach of this research, which ranged between 1.25 and 2, the mm factor was selected as 1.15 (Esfandyari et al. 2024)

2.5.1. Different manning roughness coefficient scenarios in floodplain mapping

In this study, to investigate the sensitivity of the results to the roughness coefficient for floodplain mapping, five different scenarios were considered as follows:

1) Base scenario: Manning roughness coefficient modeling was performed with values of 0.03 for the main channel and 0.05 for the left and right banks. In this scenario, hydraulic parameters including water surface elevation, maximum flow depth and velocity, water surface width, cross-sectional area, and hydraulic depth were calculated.

2) 30% increase scenario: Same as the base scenario, but with a 30% increase in the Manning coefficient.

3) 30% decrease scenario: Same as the base scenario, but with a 30% decrease in the Manning coefficient.

4) Realistic scenario (selected roughness coefficient): The roughness coefficient was selected as 0.092 for the main channel, 0.117 for the left and right banks, and 0.097 for the five downstream cross-sections (due to vegetation cover). This scenario is termed the "selected roughness coefficient" because of its proximity to the actual site conditions.

5) Effect of transversal structures: The operations of the above scenarios were repeated by incorporating the specifications of the four bridges; first, the effect of each bridge was analyzed individually, and then the combined effect of all bridges was analyzed simultaneously.

The results obtained from HEC-RAS software processing were extracted for the five scenarios as described above.

3. Results and discussion

3.1. Variations in flood discharge with different return periods, bed roughness, and the presence of bridges

The discharge variations of the main channel of the Aji-Chay River within the study reach, under the influence of floods with different return periods and various roughness coefficients, were modeled using HEC-RAS software. Furthermore, the effect of the presence or absence of bridges was investigated, and the obtained results were prepared in the form of the graph shown in Fig. 2.

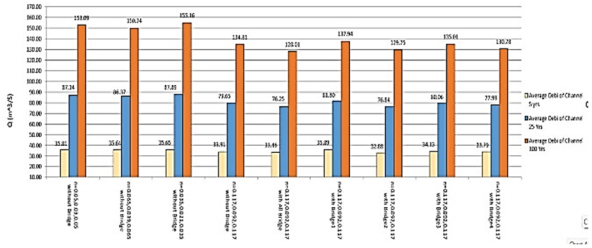


Fig. 2. Variations in average discharge of the main river channel for different return periods, various roughness coefficients, and the presence of bridges

Examining the values obtained from the results in Fig. 2, it is observed that the average discharge of the study reach, using as a baseline the scenario in which no bridge structures are present and the roughness coefficients of the left bank, bed, and right bank are 0.05, 0.03, and 0.05, respectively (Phillips and Ingersoll 1998) exhibits the following changes relative to other scenarios:

1) 30% increase in roughness coefficient: The main channel discharge decreased by 0.5%, 0.9%, and 1.9% for the 5-year, 25-year, and 100-year return periods, respectively, which is attributed to a reduction in the flow cross-sectional area. The 0.5% discharge decrease for the 5-year return period is mainly ascribed to changes in channel geometry.

2) 30% decrease in roughness coefficient: The main channel discharge decreased by 0.5% for the 5-year return period (due to flow spilling from the main channel onto the floodplains) and increased by 0.9% and 1.4% for the 25-year and 100-year return periods, respectively.

3) Selected roughness coefficient (banks 0.117, channel 0.092): The main channel discharge decreased by 5.3%, 8.6%, and 12% for the 5-year, 25-year, and 100-year return periods, respectively.

4) Selected roughness coefficient with four bridges: The main channel discharge decreased by 6.6%, 12.5%, and 14.4% for the 5-year, 25-year, and 100-year return periods, respectively.

The results and graphs for the scenario including the selected roughness coefficients (bed 0.092, left and right banks 0.117) with the effect of all bridges applied show good agreement with local conditions. The graphs related to main channel discharge, water surface width, and Froude number are presented in Fig. 3, 5, and 7, respectively.

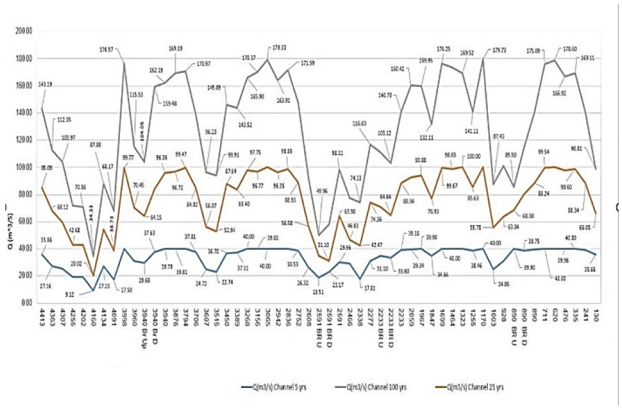


Fig. 3. Main channel discharge for different return periods with all bridges present

Comparison of the values obtained from Fig. 2 and 3 shows that the main channel discharge of the river decreased by 6.6%, 12.5%, and 14.6% for the 5-year, 25-year, and 100-year return periods, respectively. It is important to note that the reduction in main-channel discharge observed in the presence of bridge structures is a result of local flow redistribution. The hydraulic constriction caused by the bridges increases the water surface elevation, which promotes lateral flow into the floodplains. Therefore, the decrease in the main-channel flow component is physically balanced by the increased discharge within the floodplain areas, ensuring the overall mass conservation of the system under the simulated flood conditions. This reduction is attributed to the effect of bridge structures applied in the HEC-RAS software and the consequent reduction in flow cross-sectional area. Fig. 4 shows a cross-section at a distance of 3389 meters from the downstream end, where the overflow of floodwater from the main channel onto the floodplains is displayed for different return periods.

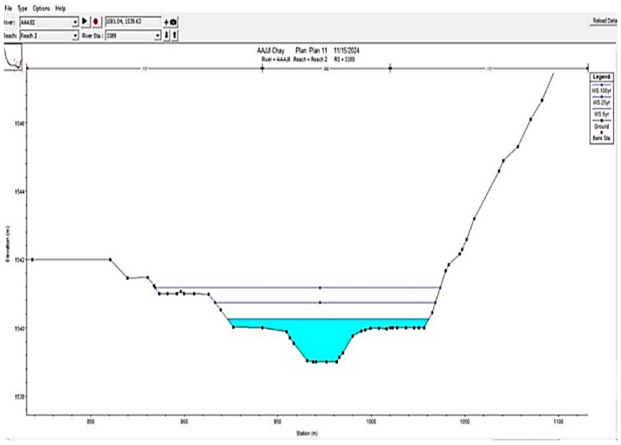


Fig. 4. Cross-section located at a distance of 3389 meters from the downstream end

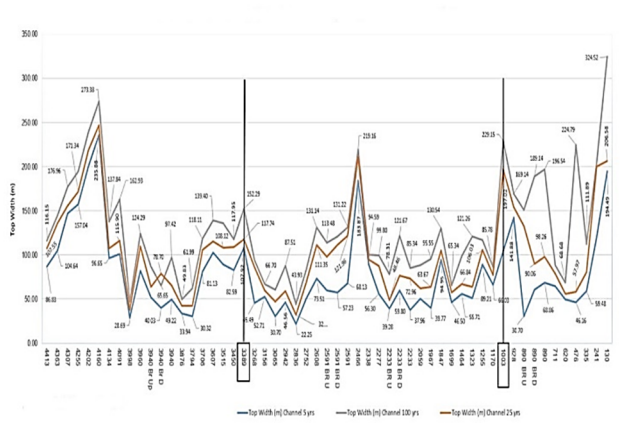


Fig. 5. Variations in water surface width for different return periods with all bridges present

Fig. 5 shows the variations in the free surface water width along the study reach. As observed, with increasing flood return period, the free surface water width increases considerably. The fluctuations in the graph at different cross-sections are also due to the geometric variations of the cross-sections. For example, at the cross-section located 1003 meters from the downstream endpoint, the free surface water width for the 100-year flood shows a significant change. Fig. 6 also depicts the free surface water elevation along the reach for different return periods. The purpose of presenting this graph is to illustrate the increasing trend of water elevation along the river course and to identify critical upstream-dominant points (such as cross-sections near bridges or abrupt changes in the riverbed). This graph enables a more accurate assessment of floodplain zoning and the determination of areas prone to overbank flow, complementing Fig. 5 in the analysis of the hydraulic behavior of the flow.

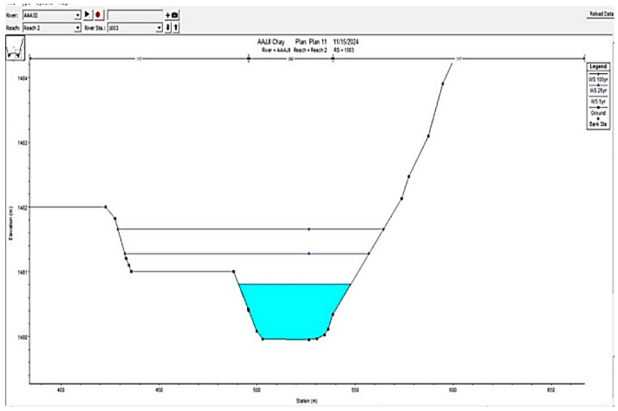


Fig. 6. Cross-section located at a distance of 1003 meters from the downstream end

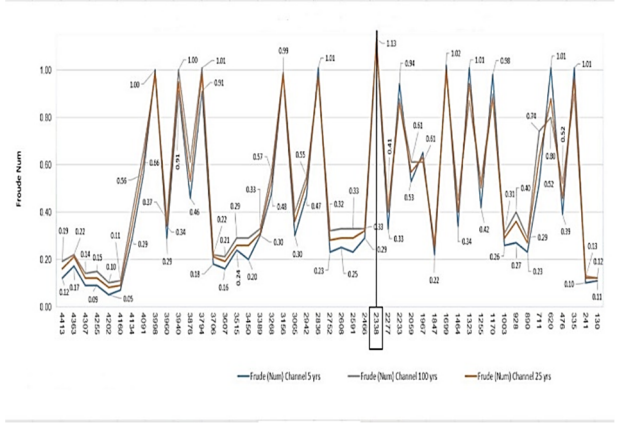


Fig. 7. Variations in Froude number for different return periods with all bridges present

In Fig. 7, it is observed that the Froude number at some cross-sections, particularly at section 3940 (adjacent to Bridge No. 1), exceeds unity, indicating supercritical flow at these points. This phenomenon can be analyzed using the Froude number equation (Equation 6) and the outputs of the HEC-RAS model.

$$F_r = \frac{V}{\sqrt{D \cdot g}} \tag{7}$$

The parameter L, representing the characteristic length, is equal to the hydraulic depth in open channels (Street 1996). The Froude number values for the cross-section located at 2338 meters from the downstream end were calculated and are presented in Table 2.

Table 2. Hydraulic results for return periods of 5, 25, and 100 years with all bridges present and the selected roughness coefficient

Station	Return period	Total discharge	Water velocity	Water area	Water surface width	Froude number
		m^3/s	m/s	m^2	m	
2338	5yr	40	1.95	25.04	88.92	1.12
2338	25yr	100	2.62	46.97	94.59	1.13
2338	100yr	180	3.16	70.95	100.35	1.13

For the 5-year return period, we have:

$$F_r = 1.95 * (0.282 * 9.81)^{-0.5} = 1.173 \quad (8)$$

With the application of the energy correction coefficient (α), the Froude number reaches 1.12. The main factor contributing to the increase in the Froude number at the cross-section located 2338 meters from the downstream end is the increase in flow velocity due to cross-section constriction near the bridge and the reduction in hydraulic depth. Furthermore, under natural conditions without the effect of transversal structures, a Froude number greater than unity is also observed. This condition typically occurs on steep slopes, narrow cross-sections, or beds with high gradients, where the flow naturally accelerates and reaches a supercritical state (Fr>1). This phenomenon underscores the importance of energy profile analysis in hydraulic design and floodplain mapping.

3.2. Analysis of cross-sections adjacent to bridges

By performing flood simulation using HEC-RAS software, the results obtained for cross-sections adjacent to bridges for different return periods indicate that, except for Bridge No. 1, the flow at the other three bridges for all return periods is subcritical. At Bridge No. 1, only during the 100-year flood does the flow become critical, with the Froude number at adjacent cross-sections reaching 1.01.

Fig. 8 shows the upstream cross-section of Bridge No. 2, where the flow for all return periods is subcritical. A significant increase in the water surface width is clearly evident for the 25-year and 100-year return periods, such that the water surface width for the 100-year flood is 124.66m, for the 25-year flood is 109.25m, and for the 5-year flood is 71.20m. The rates of increase in water surface width from the 5-year to the 25-year and from the 5-year to the 100-year return periods are 53% and 75%, respectively. This abrupt increase highlights the necessity of assessing the hydraulic capacity of the bridge and conducting detailed floodplain mapping at this cross-section. Fig. 9 presents the longitudinal profile of the entire reach along with the four bridge spans.

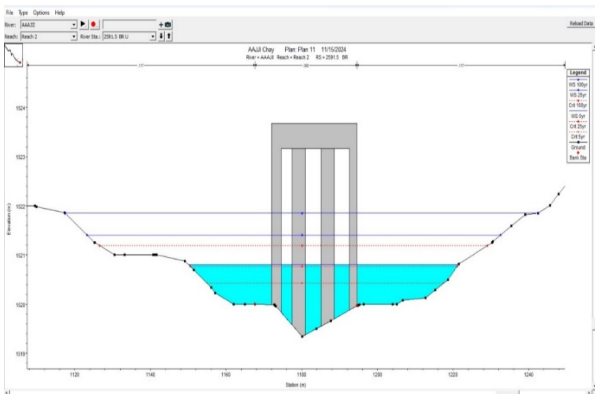


Fig. 8. Upstream cross-section of Bridge No. 2 located at a distance of 2591 meters from downstream

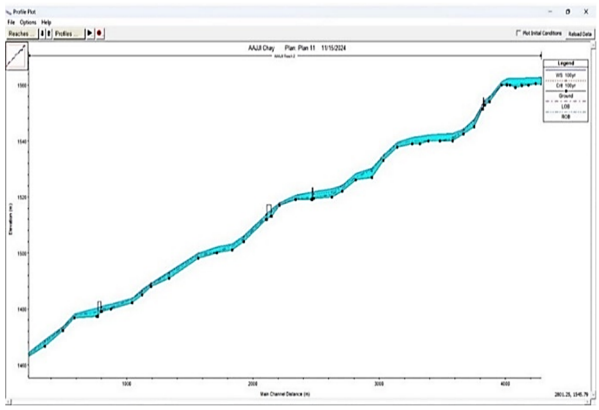


Fig. 9. Longitudinal profile of the entire river reach

3.3. Flood inundation extent for a 100-year return period with different bed roughness

The maps obtained from the software indicate that for a 100-year return period flood, as the roughness coefficient of the bed and banks increases, the extent and area of inundation in the regions adjacent to the river increase considerably. This effect is clearly observable in Fig. 10 to 12 as cross-sections at various points along the study reach; increasing roughness leads to a decrease in flow velocity, an increase in water depth, and consequently, an expansion of the floodplain extent toward the floodplains. These results emphasize the importance of accurately selecting the roughness coefficient in hydraulic modeling and floodplain mapping.

The reduction in discharge capacity observed at the bridge locations can be attributed to the hydraulic constriction effect. As the flow enters the bridge opening, the reduction in the effective cross-sectional area leads to a localized increase in velocity and a corresponding rise in the Froude number, indicating a transition toward critical flow. This constriction induces a local increase in specific energy and creates a backwater effect upstream of the structures. This mechanism, characterized by the interaction between the bridge geometry and the approaching flow, is a fundamental hydraulic response to transverse obstructions in river reaches and is consistent with the steady-state energy-based calculations performed in this study.

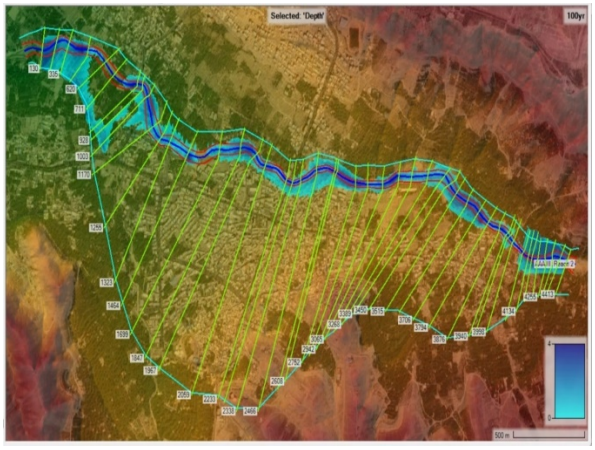


Fig. 10. Flood inundation extent for a 100-year return period with n = 0.117-0.092-0.117 (left bank-channel-right bank)

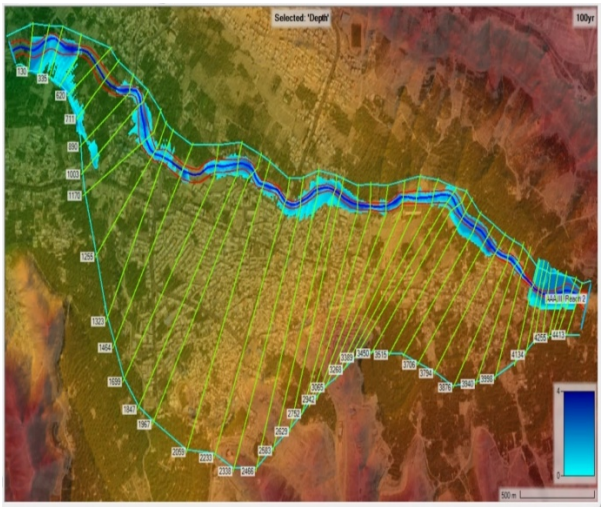


Fig. 11. Flood inundation extent for a 100-year return period with n = 0.065-0.039-0.065 (left bank-channel-right bank)



Fig. 12. Flood inundation extent for a 100-year return period with n = 0.035-0.021-0.035 (left bank-channel-right bank)

3.4. Percentage of city submersion due to flooding

To calculate the percentage of submersion of the city of Osku resulting from flood events, the inundated area of the city was computed in the RAS Mapper module of the software by measuring the perimeter of the inundated area, extracting the geographic coordinates of the points, and transferring them to Excel software. Then, using Equation (9), the total area of the city of Osku were determined, and the percentage of city submersion for floods with different return periods was obtained. The results are presented in Table 3.

$$S = \frac{1}{2}\left|\sum_{i=0}^{n-1} x_i y_{i+1} - x_{i+1} y_i\right| \quad (9)$$

Table 3. Area of the city of Osku, flood areas, and percentage of city submersion for different floods

3237773	City area of Osku exposed to inundation (excluding the river channel area)–m²
427652/62	100-year flood area-m²
377661/56	25-year flood area-m²
321566.85	5-year flood area-m²
13.21	Ratio of city submersion area for the 100-year flood (percentage)
11.66	Ratio of city submersion area for the 25-year flood (percentage)
9.93	Ratio of city submersion area for the 5-year flood (percentage)

3.5. Flood hazard assessment using the hazard index

Flow depth and velocity are among the most important parameters required for investigating flood effects. Given that the hazard index is a function of these two parameters, it is essential to numerically determine the flow depth and velocity at every point within the study area. Various definitions have been proposed for the hazard index, which are generally defined as follows:

$HR = f(h,V)$ U.S.A
$HR = f(h,v^2/2g)$ Austria
$HR = f(h,v\times h)$ Switzerland

In order to integrate the two variables of flow velocity and inundation depth in the analysis of floodplain mapping, the United States Bureau of Reclamation (USBR) introduced flood hazard curves, which allow the determination of hazard levels based on the combination of these two parameters. Using these curves, the study area is divided into three hazard zones as described below:

- **Low-hazard zone:** If the combination of flow velocity and inundation depth falls within this zone, the hazard level in the area is low, and safe passage for humans and vehicles is possible.
- **High-hazard zone:** If the combination of flow velocity and inundation depth falls within this zone, all areas in question are exposed to serious risks (including drowning, vehicle overturning, structural damage, and severe erosion).

- **Judgmental (uncertain) zone:** This zone lies between the high-hazard and low-hazard zones and defines the upper and lower hazard limits for downstream areas. In this zone, due to the specific characteristics of each flood, precise calculation of parameters is impossible. Therefore, hazard assessment in this zone depends on engineering judgment, past experiences, and field studies.

Table 4 presents the hazard index classification, and Fig. 13 shows the hazard index diagram based on USBR studies. This classification serves as an operational basis for flood risk zoning and urban crisis management.

Table 4. Classification of the hazard index

Flow velocity–depth product	Condition	Maximum flow depth (m)	Hazard index
V×h >1.5	or	h >1.5	high
0.5< V×h <1.5	or	0.5< h <1.5	medium
0.1< V×h <0.5	and	0.1< h <0.5	low

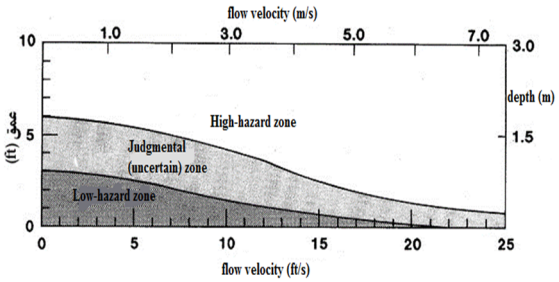


Fig. 13. Depth-velocity relationship and risk level for buildings

By examining the depth maps and the product of depth and velocity (hazard index) obtained from the RAS Mapper module, it is observed that the left bank of the river, due to its lower elevation, is exposed to greater hazard compared to the right bank. Furthermore, areas with a high hazard index are primarily concentrated along the left bank. The ratio of the area of high-hazard zones for the 100-year return period compared to the 25-year and 5-year return periods is 1.75 and 3.15 times, respectively, with calculations similar to those used for determining the inundation area. The area of high-hazard zones and their ratios to the area of the city of Osku are presented in Table 5.

Table 5. Ratio of high-hazard zone area of Osku city due to flooding

3237773	City area of Osku exposed to inundation (excluding the river channel area)-m²
128615	Area of high-hazard zones for the 100-year flood-m²
81707	Area of high-hazard zones for the 25-year flood-m²
40858	Area of high-hazard zones for the 5-year flood-m²
4	Ratio of high-hazard zone area to city area for the 100-year flood (%)
2.5	Ratio of high-hazard zone area to city area for the 25-year flood (%)
1.3	Ratio of high-hazard zone area to city area for the 5-year flood (%)

By examining Tables 4 and 5, it is observed that the percentage of inundation of the city area and the high-hazard zones of Osku city is relatively low; such that approximately 4% of the area of Osku city is classified as high-hazard zones (inundation depth greater than 1.5 meters) due to a 100-year return period flood. The ratios of city submersion area to total city area for the 100-year, 25-year, and 5-year return period floods are 13.21%, 11.66%, and 9.93%, respectively. The extents of high-hazard zones for the 100-year return period flood are shown in Fig. 14. It is worth noting that low-hazard areas (inundation depth less than 1.5 meters) are shown in blue. The other colors correspond to areas with inundation depths greater than 1.5 meters (moderate to high hazard).

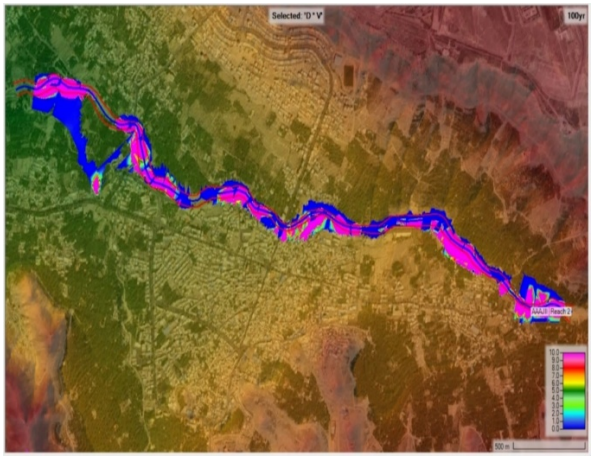


Fig. 14. Extent of high-hazard flood zones for the 100-year return period

4. Conclusion

By performing floodplain mapping and analyzing the obtained results, it was determined that the findings are in good agreement with the evidence remaining at the site. The implementation of various floodplain mapping scenarios indicated that the city of Osku is not threatened by high risk, and even under 100-year return period conditions, none of the bridges within the study reach experience flow overtopping. Furthermore, the increase in floodplain area for the 100-year flood compared to the 25-year flood is approximately 13%. Examining Fig. 2 shows that the roughness coefficient has the greatest influence on the discharge variations of the main river channel and the floodplain area, and increasing it raises the flow depth and water surface elevation. The effect of all four bridges together indicates a reduction in the

main channel discharge and floodplain extent compared to the scenario without bridges. This may be attributed to the flow approaching critical conditions, which increases flow velocity; with increased velocity, the flow cross-sectional area decreases, consequently reducing flow depth and floodplain extent. Additionally, the individual effects of the bridges, when compared with one another, show little difference in terms of river discharge and floodplain extent. However, the effect of each bridge individually, compared to the combined effect of all four bridges, does show a difference. Specifically, with only Bridge No. 1 present, the main channel discharge for the 100-year flood increases by 7.8%; with only Bridge No. 2 present, it increases by 1.4%; and with only Bridges No. 3 and No. 4 present individually, the main channel discharge for the 100-year flood increases by 5.5% and 2.2%, respectively. Therefore, it can be concluded that the presence of bridges, whether individually or collectively, reduces the main channel discharge and floodplain extent. Moreover, if the river roughness coefficient is reduced to any value lower than the selected coefficients, it will lead to a further decrease in main channel discharge and floodplain extent. From the results obtained, it is inferred that the inundated area of Osku city is 427,650m², equivalent to 13.21% of the city's total area. Furthermore, the area of high-hazard zones for the 100-year flood, with inundation depths of 1.5 meters or more, is 128,615 m², covering approximately 4% of the city's total area. Of this, 1.28% comprises residential areas, 0.68% corresponds to the road leading to the village of Fesghandis, 0.36% consists of warehouses and small technical-industrial workshops, and the remaining 1.68% includes orchards and riverside villas. Additionally, the remaining traces of the high-water mark (Daghāb line) from past floods, located between cross-sections at 3156 and 3065 meters from the downstream end, confirm the accuracy of the results and the magnitude of the flood discharge. Field observations along the study reach indicated that human activities have introduced significant morphological changes to the river. These activities include encroachment upon the river buffer zone and residential construction adjacent to the river, dumping of municipal and construction waste, installation of urban facilities such as electricity poles and municipal sewage manholes, and, in some areas, localized bed material extraction. All these factors contribute to increasing the river's roughness coefficient and reducing its cross-sectional area, which, in the event of a flood, would cause damage to local residents. Furthermore, the discharge of wastewater entering the river in the vicinity of Bridges No. 1 and No. 3 pollutes the riverbed and the local environment. It is essential that relevant government authorities take action to organize and optimize the dimensions and bed of the river, prevent the dumping of municipal and construction waste, and thereby stabilize the riverbed while preventing pollution and potential disease outbreaks in the city. Additionally, the fire station and the Water Affairs Office of Osku city are located within the 25-year floodplain. Given the emergency response nature of the fire station during critical situations, relocating it is deemed necessary.

It is recommended that urban management and water resources authorities adopt long-term measures to optimize the riverbed and reduce encroachments upon the river buffer zone. By enforcing the 25-year floodplain as the river buffer zone in accordance with the regulations pertaining to “Riverbeds and Buffer Zones” issued in 2000 (Iranian calendar year 1379), encroachment by the public can be prevented, and a structured plan should be implemented to deter unauthorized activities by individuals.

4.1. Limitations

It should be noted that the model results were qualitatively verified against historical flood marks and observed inundation extents to ensure the spatial plausibility of the simulated patterns. Due to the unavailability of high-precision, surveyed water-level data from previous flood events in the Aji-Chay River, a quantitative statistical validation (e.g., RMSE or R^2) was not performed. Consequently, the results should be interpreted as a qualitative assessment of the flood extent and potential risk areas.

It should be noted that the current study employs a steady-state 2D modeling approach to evaluate the peak inundation extent and flow redistribution caused by the bridge structures. While this approach is effective for assessing the hydraulic capacity under peak conditions, it does not account for the temporal variations of the flood wave. Therefore, future research should incorporate unsteady-state simulations to capture the dynamic progression of flood waves and their attenuation effects over time.

5. References

Abbaszadeh H, Daneshfaraz R, Sume V, Abraham J, “Experimental investigation and application of soft computing models for predicting flow energy loss in arc-shaped constrictions”, AQUA-Water Infrastructure, Ecosystems and Society, 2024, 73 (3), 637-661. https://doi.org/10.2166/aqua.2024.010

Arcement GJ, Schneider VR, Guide for selecting Manning’s roughness coefficient for natural channels and flood plains (U.S. Geological Survey Water-Supply Paper 2339, pp. 2-10), 1989, U.S. Geological Survey.

Coon WF, “Estimation of roughness coefficients for natural stream channels with vegetated banks (U.S. Geological Survey Open-File Report 93-161)”, 1995: New York State Department of Transportation / U.S. Geological Survey.

Daneshfaraz R, Norouzi R, Abbaszadeh H, Azamathulla HM, "Theoretical and experimental analysis of applicability of sill with different widths on the gate discharge coefficients", Water Supply, 2022, 22 (10), 7767-7781. https://doi.org/10.2166/ws.2022.354

Eftekhari A, Sadeglou T, Ahmadabadi A, Sojasi H, "Evaluating flood zoning of Gorganroud River basin by considering villages at flood risk using HEC RAS model", Rural Development Journal, 2009, 1 (1).

Esfandyari Dorabad F, Mostafazadeh R, Naseri A, "Determination of meander pattern in gharehsou river using sinuosity coefficients and central angle in anzab-samian bridge reach", Journal of Applied Researches in Geographical Sciences, 2021, 21 (61), 7. http://dx.doi.org/10.52547/jgs.21.61.119

Hasanzadeh Y, Keynejad MA, Roushangar K, Tagi Alami M, "One-dimensional simulation of flow and sediment transport, a case study in the aland river", Journal of Water and Wastewater, 2010, 21 (1), 4-14.

Hassanzadeh Y, Kardan N, Arzanlou A, "Numerical simulation and flood zoning by two-dimensional model", In Proceedings of the 3rd National Hydrology Conference of Iran, 2019, University of Tabriz, Iran.

Hassanzadeh Y, "Engineering and management of flood control and dambreak", Tabriz University Publications, 2024.

Iran National Cartographic Center, [Untitled-Journal of the Faculty of Natural Resources, University of Tehran, 3], 2006, Mehr 1385 [Iranian Calendar].

Kardan N, Hassanzadeh Y, Arzanlou A, "Two-dimensional simulation of urban flood by CCHE2D model: A case study in Aghgola city, Golestan province", Marine Technology, 2018, 4 (4), 25-36.

Phillips JV, Ingersoll TL, "Verification of roughness coefficients for selected natural and constructed stream channels in Arizona (U.S. Geological Survey Professional Paper 1584), 1998: U.S. Geological Survey.

Planning and Budget Organization issues No. 592 643 688, 2022.

Pornaby Darzi S, Vafakhah M, Rajabi MR, "Flood hazard zoning using HEC-RAS hydraulic model and ArcGIS (Case study: Cheshmeh-Kileh River in Tonekabon county)", Journal of Natural Environmental Hazards, 2021, 10 (28), 15-28.

Street RL, "Elementary fluid mechanics (7th ed.)", Wiley; 1996.

USBR ACER TM11. "Downstream hazard classification guidelines", Assistant Commissioner of Denver, Colorado, 1988.